
Cylinder-Pressure-Based Engine Control Using Pressure-Ratio-Management and Low-Cost Non-Intrusive Cylinder Pressure Sensors

Mark C. Sellnau

Delphi Central Research and Development

Frederic A. Matekunas, Paul A. Battiston and Chen-Fang Chang

General Motors Research and Development Center

David R. Lancaster

General Motors Powertrain Group

Reprinted From: **Electronic Engine Controls 2000: Controls
(SP-1500)**

The appearance of this ISSN code at the bottom of this page indicates SAE's consent that copies of the paper may be made for personal or internal use of specific clients. This consent is given on the condition, however, that the copier pay a \$7.00 per article copy fee through the Copyright Clearance Center, Inc. Operations Center, 222 Rosewood Drive, Danvers, MA 01923 for copying beyond that permitted by Sections 107 or 108 of the U.S. Copyright Law. This consent does not extend to other kinds of copying such as copying for general distribution, for advertising or promotional purposes, for creating new collective works, or for resale.

SAE routinely stocks printed papers for a period of three years following date of publication. Direct your orders to SAE Customer Sales and Satisfaction Department.

Quantity reprint rates can be obtained from the Customer Sales and Satisfaction Department.

To request permission to reprint a technical paper or permission to use copyrighted SAE publications in other works, contact the SAE Publications Group.



GLOBAL MOBILITY DATABASE

All SAE papers, standards, and selected books are abstracted and indexed in the Global Mobility Database

No part of this publication may be reproduced in any form, in an electronic retrieval system or otherwise, without the prior written permission of the publisher.

ISSN 0148-7191

Copyright © 2000 Society of Automotive Engineers, Inc.

Positions and opinions advanced in this paper are those of the author(s) and not necessarily those of SAE. The author is solely responsible for the content of the paper. A process is available by which discussions will be printed with the paper if it is published in SAE Transactions. For permission to publish this paper in full or in part, contact the SAE Publications Group.

Persons wishing to submit papers to be considered for presentation or publication through SAE should send the manuscript or a 300 word abstract of a proposed manuscript to: Secretary, Engineering Meetings Board, SAE.

Printed in USA

Cylinder-Pressure-Based Engine Control Using Pressure-Ratio-Management and Low-Cost Non-Intrusive Cylinder Pressure Sensors

Mark C. Sellnau

Delphi Central Research and Development

Frederic A. Matekunas, Paul A. Battiston and Chen-Fang Chang

General Motors Research and Development Center

David R. Lancaster

General Motors Powertrain Group

Copyright © 2000 Society of Automotive Engineers, Inc.

ABSTRACT

Over the last two decades, advanced engine control systems have been developed that use cylinder pressure as the primary feedback variable. Production application has been limited by cost, reliability, and packaging difficulties associated with intrusive cylinder pressure sensors. Now, a low-cost cylinder-pressure-based engine control system has been developed that utilizes Pressure-Ratio Management (PRM) and non-intrusive cylinder pressure sensors mounted in the spark plug boss of four-valve-per-cylinder engines. The system adaptively optimizes individual-cylinder spark timing and air-fuel ratio, and overall exhaust gas recirculation (EGR) for best fuel economy and lowest emissions over the life of each vehicle.

This paper presents the engine control and cylinder pressure sensor systems. Results are presented showing spark timing and EGR control, knock and misfire detection, cylinder-to-cylinder air/fuel balancing, and cold start control.

INTRODUCTION

Development of advanced engine control systems for the modern 4-stroke gasoline engine is being driven by demand for higher fuel economy and increasingly stringent exhaust emissions standards. Additionally, emissions compliance must be maintained for increasing service duration while On-Board-Diagnostics (OBDII) requirements are satisfied.

Individual-cylinder, cylinder-pressure-based feedback control is an ideal method to optimize engine operation [1, 2] (numbers in brackets indicate references found at the end of this paper) over vehicle life while fulfilling diagnostics requirements. Cylinder pressure is a fundamental combustion variable, which can be used to characterize the combustion process for each combustion event. Optimal engine control can be maintained by monitoring the pressure in each cylinder and using this information for feedback control of spark timing, exhaust gas recirculation (EGR), air-fuel ratio (A/F), and combustion knock. The system is not proposed, however, as a replacement for stoichiometric A/F control using an oxygen sensor, however, for lean systems, such replacement has been demonstrated.

The ability to sense and adapt for factors that produce deviations from the best open-loop calibration yields a wide range of benefits. These benefits are summarized in Tables 1 and 2 below. Fuel economy may be increased and nitrogen oxide (NOx) emissions decreased by operation with higher levels of EGR or with leaner A/F ratios than would normally be practical. Further efficiency gains result by operation of each cylinder at Minimum Spark Advance for Best Torque (MBT), thereby compensating for burn rate and spark requirement differences from cylinder-to-cylinder. Cylinder-pressure-based control can adapt for environmental factors, component manufacturing variations, component wear, and component degradation of various types, effectively reducing exhaust emissions dispersion and deterioration for an aging fleet. Cold start fueling algorithms that are based on cylinder pressure measurements may substantially reduce exhaust hydrocarbon (HC) emissions.

Table 1. Primary System Benefits for Cylinder-Pressure-Based Engine Control

Primary Benefits	Description
<i>Fuel Economy</i>	<i>Increased exhaust gas recirculation (EGR) reduces pumping work and improves gas properties; individ. cyl. spark timing optimizes each cyl.; MBT spark advance avoids fuel economy loss from spark retard.</i>
<i>NOx Emissions</i>	<i>Increased EGR levels beyond normally practical levels with MBT spark timing.</i>
<i>Hot HC Emissions</i>	<i>Hot HC emissions may be reduced by lean exhaust biasing and the associated increased catalyst HC conversion efficiency.</i>
<i>Cold HC Emissions</i>	<i>Air-fuel ratio control during the cold start enables leaner A /F ratios for reduced HC emissions. Precise retard control improves catalyst heating.</i>

Table 2. Secondary System Benefits for Cylinder-Pressure-Based Engine Control

Secondary Benefits	Description
<i>Misfire Detection</i>	<i>Cylinder pressure provides outstanding misfire and partial burn detection for the full engine operating range.</i>
<i>Knock and Pre-ignition Detection</i>	<i>Improved knock detection and pre-ignition detection enables aggressive MBT spark calibrations for improved engine torque and efficiency. Eliminates “false retards”. Replaces knock sensor(s).</i>
<i>Air-Fuel Balancing</i>	<i>Improves Dilution Limit and yields improved A/F-control, reducing fleet emissions, and emissions dispersion and deterioration.</i>
<i>Calibration Assist</i>	<i>Simplifies and reduces calibration requirements for “fast to market” and “niche” markets.</i>
<i>Service Diagnostics</i>	<i>Detect and diagnose a variety of component failures on-board. Improve service effectiveness. Improve customer satisfaction.</i>
<i>Warranty Reduction</i>	<i>Compensation for component degradation. Accurately detect component failures; reduce “no trouble found” occurrences.</i>
<i>Camshaft Phasing</i>	<i>Determines active cylinder (Cylinder ID) immediately upon cranking. Replaces cam sensor.</i>

Improved detection of combustion knock and pre-ignition enables safe operation closer to MBT spark advance, while cylinder pressure sensing provides outstanding detection of misfire and partial burn cycles for the full range of engine operating conditions. As future automotive engine systems become more complex, cylinder-pressure-based control enables reduced dependency on expanding open-loop calibrations and may simplify calibration requirements while speeding the overall calibration process.

A variety of cylinder-pressure-based engine control systems has been reported in the literature [3,4,5,6]. Generally, cost, packaging, and durability considerations have limited production applications of these systems. Some systems have also been compromised by poor sensor signal quality or algorithm design, both of which may limit system performance and functionality, and reduce system benefits.

The most common type of cylinder pressure sensors are intrusive devices that package through the combustion chamber wall [7-20]. While intrusive sensors are evolving into smaller designs, production viability of packaging these sensors within the crowded space of an engine cylinder head remains a formidable challenge throughout

the industry. Cost of these devices is generally high and the hostile thermal and mechanical environment of the combustion chamber introduces serious durability concerns.

Non-intrusive sensors [21-35] do not require direct access to the combustion chamber. Pressure is detected indirectly by sensing stress in an existing engine component (e.g., head bolt). Because of their integration into existing components, non-intrusive devices are generally lower cost than intrusive sensors. However, signal quality depends strongly on the mechanical load path of the resulting package and is often below requirements. In-spark-plug devices [36-43] have been of interest since they do not require an additional access port to the combustion chamber. Significant engineering resources have been applied recently to develop an integrated spark plug pressure sensor as part of the ignition subsystem. Unfortunately, use of piezoelectric, fiber optic, or magnetostrictive sensing technology has not resulted in a practical, low-cost, in-spark-plug device.

Algorithms for cylinder-pressure-based engine control have been developed with various control functionality, and pressure sensor, sampling, and processing requirements. Location of Peak Pressure (LPP) [44-53] is

a well-known algorithm that is relatively easy to implement and does not require calibrated sensors. For strong mixtures, control of LPP to a predetermined MBT target can provide effective spark-timing control. This approach has reduced applicability for dilute mixtures, such as at idle or for high EGR rates, and can not be used effectively for control of EGR, A/F, or other engine control variables [53].

Indicated mean effective pressure (IMEP) may be calculated by sampling the cylinder pressure waveform during the combustion event. Toyota produced an engine control system [54,55] based on this approach using a single intrusive pressure sensor mounted in cylinder #1. Cylinder pressure measurements were sampled four times during the expansion stroke as an estimate of IMEP. JECs also developed a similar system on a 3.0l V6 using a spark plug load washer in each cylinder [56]. The algorithm is useful for monitoring engine torque fluctuations for indication of combustion dilution limits [57,58,59] and for detection of misfired cycles. However, IMEP has limited application for other engine control functions.

An empirical method called the “moment algorithm” [60,61,62] was developed to estimate the mixture A/F ratio by applying pattern recognition techniques to the cylinder pressure waveform. The “shape information” contained in the cylinder pressure waveform was quantified by calculating the first, second and third moments of pressure vs. crank angle, and using these as inputs to an estimator algorithm. The gain and bias of the pressure sensor were not required and a reasonable correlation between A/F and engine variables was demonstrated. The calculation procedure, however, was computationally intensive and was not extended to other control functions such as spark timing control.

Another approach to engine control using cylinder pressure is the “difference pressure” technique developed by Bosch [18, 63,64]. The difference pressure (DP) is defined as the difference between the measured combustion pressure and the calculated motored pressure for the same cycle. The difference pressure integral (DPI) is the integral of DP between top-dead-center (TDC) and 180 crank-angle-degrees (CAD) after-top-dead-center (ATDC) and was used for misfire detection, spark timing control, and dilution limit detection. The algorithm offers the benefit of insensitivity to pressure sensor bias but conversely, requires a sensor with known gain (calibrated).

It is generally recognized that excellent measures of knock intensity may be obtained from cylinder pressure measurements, depending on the pressure sensor type and mounting location within the engine [1,65,66,67]. Nissan produced a system on a 3.0l V6 that used ring load washers mounted under each spark plug to detect individual-cylinder combustion knock [34,35]. Owing to improved knock detection from cylinder pressure measurements, knock system performance can be improved and the knock calibration may be simplified.

The current work offers a new solution to the technical and commercial limitations of other pressure-based engine control systems. The technology developed reduces the cost and complexity historically associated with cylinder-pressure-based engine control systems, while providing increased control functionality. The control algorithm used is based on fundamental combustion principles, is computationally efficient, and greatly reduces requirements on the pressure sensor system. The pressure sensor used is a piezoelectric, non-intrusive device that has potentially excellent durability with estimated cost between one half to one quarter the cost of competitive intrusive sensors. This paper presents the control system, control algorithms, and the sensor system. Test results for spark-timing control, dilution control, A/F balancing, misfire and knock detection, and the cold start are shown. Improvements in vehicle fuel economy, NOx emissions, and HC emissions are reported.

PRESSURE-RATIO MANAGEMENT

FUNDAMENTAL PRINCIPLES – Rassweiler and Withrow [68] showed that the mass burn fraction (MBF) for an engine could be determined from the fractional pressure rise due to combustion. The algorithm used in the current work is based on this principle and is called Pressure-Ratio Management (PRM) [69,70,71]. For each combustion event, the algorithm provides determination of combustion phasing and combustion dilution.

To illustrate PRM, the fired cylinder pressure and the “motored pressure” that would exist if combustion did not occur are shown in Figure 1a. The pressure ratio (PR) is defined as the fired pressure divided by the motored pressure and is shown in Figure 1b.

$$PR(\theta) = P(\theta) / P_{\text{mot}}(\theta) \quad (1)$$

The PR has unity value before combustion and rises during combustion to a final pressure ratio (FPR) which depends on the amount of heat release per unit charge mass. The increase in the final pressure ratio is called the modified pressure ratio, MPR.

$$MPR = FPR - 1 \quad (2)$$

The fractional rise in the pressure ratio is an estimate of the mass burn fraction. The accuracy of the estimate is influenced only slightly by heat transfer and piston motion [70]. Since the pressure ratio is, by definition, a ratiometric measure of cylinder pressures, PRM algorithms do not require the gain of the pressure sensor. The bias of the pressure signal (voltage) is computed using two compression samples with the assumption of polytropic behavior [70]. Therefore, PRM is inherently insensitive to many of the common errors in pressure measurement. Importantly, this enables use of low-cost pressure sensors for practical implementations of the system.

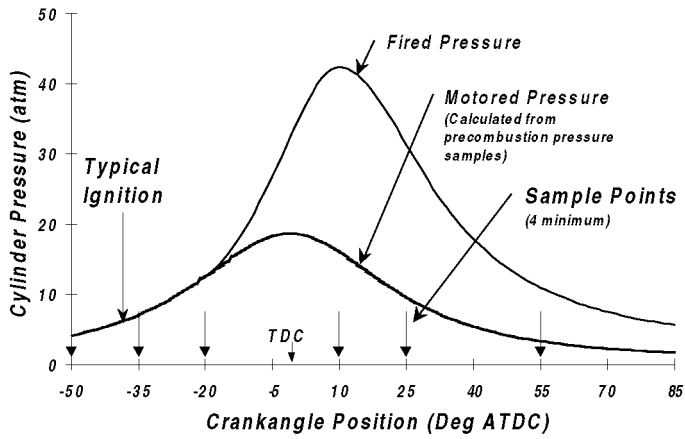


Figure 1a. Fired and Motored Cylinder Pressures.

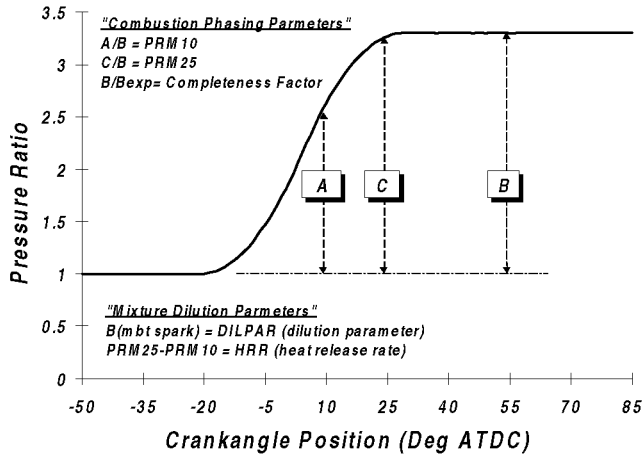


Figure 1b. Pressure Ratio Curve.

PRESSURE SAMPLING REQUIREMENTS – Implementation of PRM requires pressure sampling at a minimum of 4 discrete crank angle locations for which cylinder volume is known. Two samples are taken prior to significant heat release (typically 35 and 50 degrees before-top-dead-center (BTDC)) for determination of the motoring pressure waveform and the signal bias from polytropic relationships (see Figure 1a). A sample taken after combustion is complete (typically 55 degrees ATDC) is needed to determine the FPR, which is represented as quantity B in Figure 1b. A sample taken at 10 degrees ATDC (during combustion) provides the pressure ratio at this point. The fractional rise in pressure ratio is an estimate of the mass burn fraction. For the 10 degree ATDC point, this is represented by the quantity A/B in Figure 1b and is also called the PRM timing parameter, PRM10.

PRM10 TIMING PARAMETER – The PRM10 timing parameter is a very sensitive measure of combustion phasing and is useful for MBT spark timing control.

$$PRM10 = [PR(10) - 1] / [FPR - 1] \quad (3)$$

PRM10 values range between 0 and 1. For spark-ignited engines, MBT spark timing yields a PRM10 value of about 0.55 under all operating conditions. Retarded

spark timing yields lower values of PRM10; advanced timing yields higher values of PRM10. Typically, a change of 0.1 in PRM10 corresponds to 3 to 5 degrees change in spark timing. Because the mass burn rate and the slope of the PR curve are near their maximum at 10 degrees ATDC, the PRM10 parameter remains a sensitive measure of combustion phasing even for high dilution ratios.

PRM techniques may be extended for special operating modes that require control of late combustion phasing. Spark timing is commonly retarded during cold starts for catalyst heating, and transmission shift control can be improved by momentary spark retard for engine torque reduction. A PRM25 timing parameter is defined for this purpose and is illustrated in Figure 1b. The PRM25 timing parameter requires an additional pressure sample at 25 degrees ATDC.

FINAL PRESSURE RATIO AND DILPAR DILUTION PARAMETER – Final pressure ratio is a measure of the combustion heat release per unit charge mass. For combustion with MBT spark timing, FPR is a maximum for stoichiometric mixtures with no dilution, and decreases as excess air, EGR, or residuals are increased. Therefore, FPR is useful as an indicator of total charge dilution, and is applicable to the control of mixture dilution in systems which are lean burn, use high amounts of EGR, or vary the amount of residual through variable valve train systems. For spark-ignited engines with MBT spark timing, FPR has a typical range between 2.8 and 4.0.

$$FPR = PR(55) \quad (4)$$

FPR is sensitive to combustion phasing due to cycle heat losses [70]. Early combustion phasing causes lower FPR, and visa versa. Fortunately, in the interest of obtaining a pressure-based dilution parameter solely dependent on dilution, this phasing dependency is approximately linear with PRM10 and may be readily corrected. As a result, the FPR that would have existed if the cycle burned at MBT may be determined. This quantity is called the Dilution Parameter, or DILPAR.

$$DILPAR = FPR + (0.5 * PRM10) - 1.275 \quad (5)$$

DILPAR provides an estimate of total charge dilution for any one cycle that burns completely. DILPAR exhibits lower cyclic variability than FPR (or MPR), which include the effects of combustion phasing. Since the total charge dilution that a combustion system can tolerate remains nearly constant over the full operating range, DILPAR is a very useful estimator for combustion control with lean A/F ratios or high EGR.

ENGINE CONTROL STRATEGIES BASED ON PRM – From this understanding of the pressure ratio and its use to characterize the combustion process, a variety of engine diagnostic and control strategies have been

conceived. The overall engine control strategy for this system was to deliver EGR near the dilution limit, optimize individual-cylinder spark timing, and balance A/F ratio, adaptively, for maximum fuel economy and minimum emissions over the life of each vehicle.

Closed-loop, MBT, spark-timing control may be achieved by controlling PRM10 to a nominal target value of 0.55. To implement this overall scheme, the required accuracy of PRM10 is about ± 0.05 . Pressure sensor accuracy corresponding to this level of PRM10 accuracy is presented in the next section. Modifications to the PRM10 target value of 0.55 may be performed to control combustion knock and pre-ignition, or for spark retard during decels and the cold start. These applications are discussed further in following sections.

Closed-loop EGR control may be implemented using three different control strategies as summarized below:

Method 1 Dilution Control – Control DILPAR to a target value based on known dilution limits of the engine. This method to control dilution is illustrated in Figure 2a and requires the greatest accuracy on DILPAR (± 0.05).

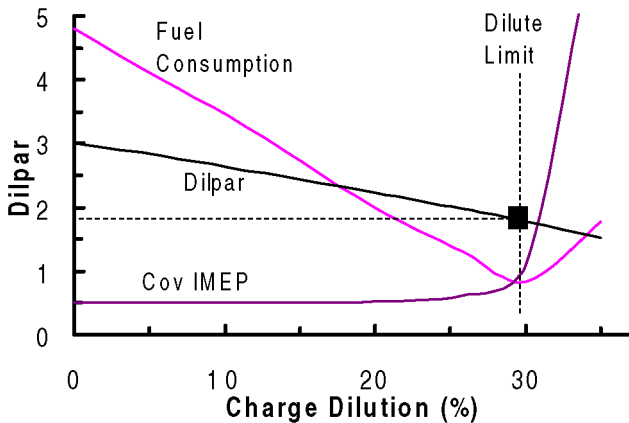


Figure 2a. Method 1 Dilution Control

Method 2 Dilution Control – The spark timing required to produce a given value of PRM10 indicates charge dilution. Using this fact, dilution may be controlled by maintaining PRM10 at 0.55 and varying EGR until a spark-timing target is reached. Spark timing targets are based on known dilution limits of the engine, which correspond to the best efficiency mixtures. The advantage of this method is that it is less sensitive to pressure measurement errors than Method 1. PRM10 accuracy of ± 0.05 is typically required. This method of dilution control is illustrated in Figure 2b.

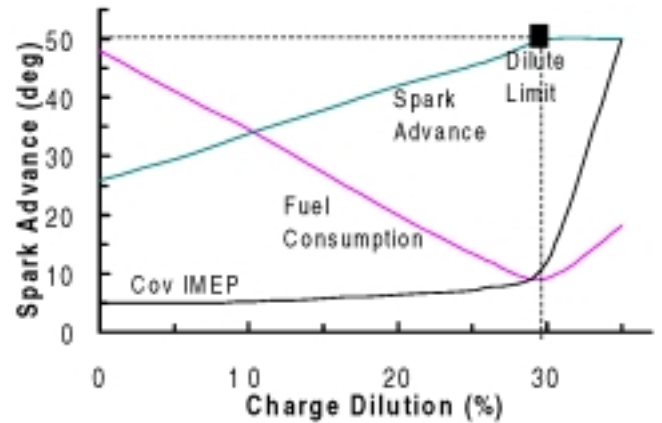


Figure 2b. Method 2 Dilution Control

Method 3 Dilution Limit Detection (DLD) – Typically, the dilution limit is indicated by both a covariance of indicated mean effective pressure (COV of IMEP) of about 3 percent and the onset of partial-burn cycles. The dilution limit may be detected by measuring the variability of DILPAR (or MPR) and monitoring for partial-burn cycles. This method requires the least accuracy on DILPAR (± 0.3) and is illustrated in Figure 2c.

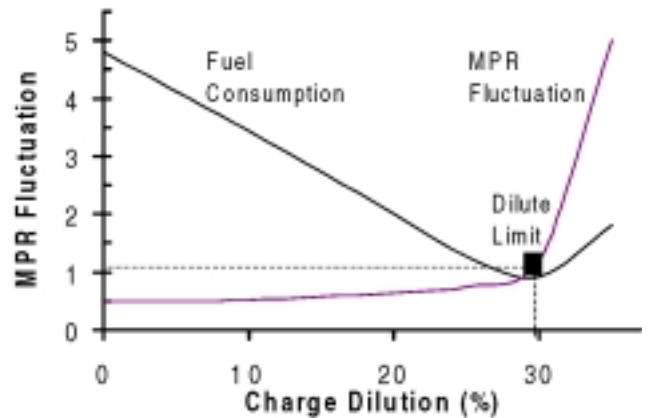


Figure 2c. Method 3 Dilution Limit Detection

For the current work, Method 2 and Method 3 were selected for dilution control since they provide the greatest robustness with the least sensitivity to pressure measurement errors. By combining these two methods, an engine may be operated as dilute as practically possible while avoiding torque instability problems. For partial burn detection (i.e. at the dilution limit), MPR was used as an indicator of total heat release per cycle. This method will be presented in more detail in the section on Misfire Detection. Use of Pressure-Ratio Management for A/F balancing and cold start fuel control will also be presented in following sections.

CYLINDER PRESSURE SENSING SYSTEM

Successful implementation of pressure-based engine control using PRM depends on availability of a production-viable cylinder pressure sensor that satisfies cost, packaging, and reliability requirements. The sensor must respond sufficiently linearly to cylinder pressure during the sampling window (-50 to 70 degrees ATDC), however, only a relative measure and not an absolute measure of pressure is required. This means that sensor gain and bias changes are permitted as long as these changes occur below a certain rate.

To meet these requirements, a new pressure-sensing concept [72] was conceived and developed. The sensor is a non-intrusive device called the “spark-plug-boss” (SPB) cylinder pressure sensor. The sensor uses piezoelectric sensing technology to detect compressive forces in the cylinder head structure in response to cylinder gas pressure loading. Mounting of the sensor in a four-valve-per-cylinder engine is shown in Figure 3. A photograph and cross sectional drawing of the sensor are shown in Figures 5 and 6.

SENSOR LOAD PATH DESCRIPTION – The SPB pressure sensor operates in a structural load path that is very linear and well behaved. Cylinder pressure acting on the combustion chamber creates a force that is elastically transferred through the cylinder head structure to the head bolts. A portion of this total force is transferred in compression through the spark plug boss and has a magnitude of about 2200 N at maximum cylinder pressure (6.8 MPa). This provides a reasonable but not excessive force for sensing. To detect the force, a shoulder is machined on the inner diameter of the spark plug boss and the sensor is preloaded onto the shoulder using fastening threads. To accommodate the sensor, the cast outer diameter of the upper spark plug boss is increased about 6 mm. Because the sensor is located high within the spark plug boss, the sensor has no detrimental effect on spark plug cooling. The sensor is responsive to compressive forces applied through the sensor bottom face (see Figure 3).

A detailed thermal-structural analysis for the sensor and cylinder head was performed to confirm load path sensitivity to cylinder pressure and insensitivity to extraneous loads (Figure 4). Various extraneous loads are known (valve train dynamics, thermal loads, etc), however, since loads caused by cylinder pressure are large, tests show that error signals could be effectively isolated and minimized (see section on signal validation). Frequency response of the installed sensor is about 20 kHz, which is adequate for detection of cylinder pressure including combustion knock.

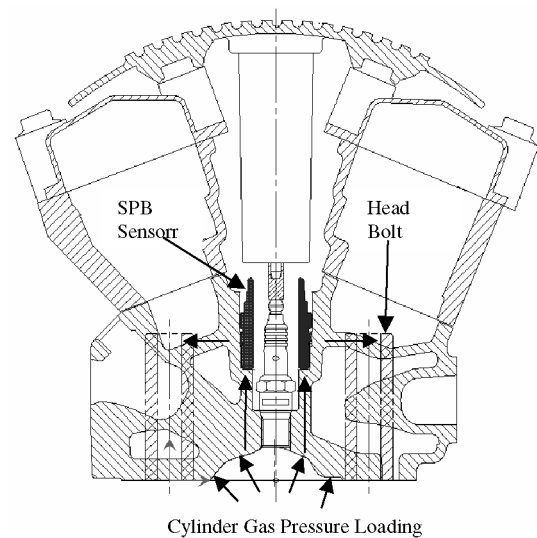


Figure 3. Spark-Plug-Boss Sensor Installed in 4-Valve-per-Cylinder Engine (Connection System Not Shown).

The advantages of this overall sensing concept are:

1. Direct access to the combustion chamber is not required
2. Due to abundance of cooling water surrounding the spark plug boss, sensor operating temperatures and hot soak temperatures are relatively low (140 C maximum).
3. Due to mounting outside of the combustion chamber, the sensor is insensitive to several common types of thermal errors including intracycle flame arrival effects and signal drift during engine load transients.

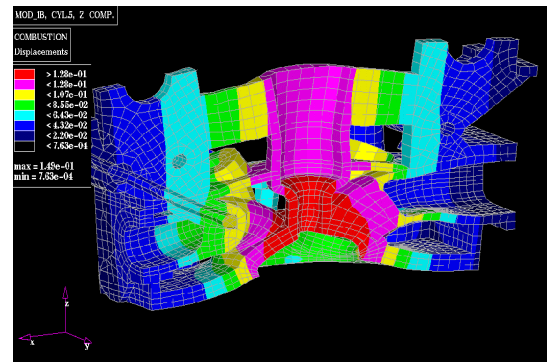


Figure 4. Structural Analysis of Cylinder Head Demonstrates Maximum Displacement at Chamber Centerline (Cylinder Pressure Loading)

Table 3. SPB Cylinder Pressure Sensor Specifications for Use with PRM.

Parameter	Value	Units
Operating Conditions		
Operating Temperature Range	-55 to 150	C
Maximum Exposure Temperature	200	C
Working Cylinder Pressure Range	0 to 8.3	MPa
Burst Pressure	13	MPa
Pressure Sensitivity and Linearity		
Pressure Sensitivity (nom.)	0.92 +/- 0.27	mV/kPa
Force Sensitivity to Pressure (typ.)	90 to 120	N/MPa
Hysteresis and Non-Linearity Combined	+/- 3.0	% of FS
Mechanical Characteristics		
Sensor Static Preload Range	3300 to 11000	N
Dynamic Load (at max. pressure, nom.)	1100	N
Installation Torque Range	40 – 55	Nm
Frequency Response	~20	kHz
Electrical Characteristics		
Constant Current Input	1.0 – 2.0	mA
Supply Voltage	11 – 16	V
Power Supply Noise Rejection	30	dB
Output Voltage Range	0 – 10	V
Low-Frequency Cutoff (3 dB down)	0.1 to 0.2	Hz
High-Frequency Cutoff (3 dB down)	28 to 32	kHz
Output Ground Insulation (min.)	2	Mohm
Output Capacitance (max.)	100	pF
Power-Up Delay (from “key on”)	75	ms

Design specifications for the Spark-Plug-Boss Sensor used with Pressure-Ratio Management are listed in Table 3. An error sensitivity analysis was performed to determine some of the specifications in Table 3. The values listed may be adapted to suit specific engine control applications.

SPARK-PLUG-BOSS CYLINDER PRESSURE SENSOR – Referring to Figures 5 and 6, The Spark-Plug-Boss Sensor is a simple force transducer with an annular cross sectional shape. The inner diameter of the sensor equals the diameter of the spark plug well. The sensor is comprised of six components arranged on a single axial centerline [73]. This enables low-cost assembly of the sensor using automated tools and procedures. A deep-drawn aluminum can shields the sensor assembly on the inner diameter. The assembly is sealed hermetically using dispensed silicone sealants.

Mechanical loads acting on the sensor are transferred upward in compression through the sensor shield, the protection washer, and the piezoceramic element to the threaded shell. The fastening threads on the shell are a 5-degree buttress design that align thread loads axially for linear load transfer characteristics [74]. To minimize thermal-induced error signals, the shell is fabricated from high-strength aluminum alloy, which has a coefficient of

thermal expansion equal to that of the aluminum cylinder head. The shell is nickel plated to prevent thread galling and corrosion.



Figure 5. Spark-Plug-Boss Cylinder Pressure Sensor

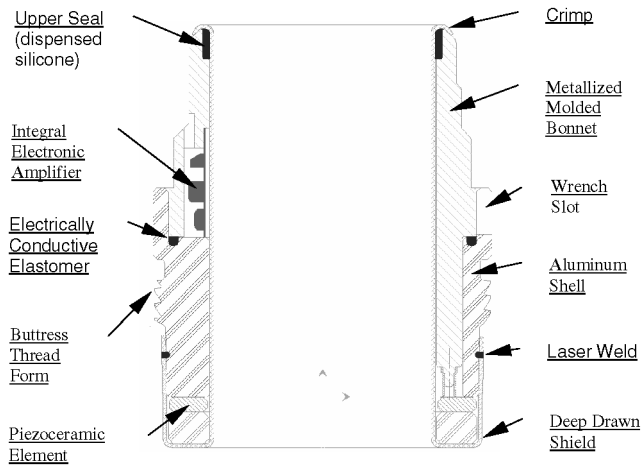


Figure 6. Cross Sectional view of SPB Sensor

The piezoceramic element generates a charge signal proportional to the applied dynamic force. The charge signal is conducted along a metalized trace on the bonnet to an integral electronic amplifier located on the bonnet inner diameter. The amplifier converts the charge signal into a low-impedance voltage signal. The voltage signal (output) is conducted through a metalized through-hole to an annular output terminal on the bonnet outer diameter. This permits installation of the sensor in any rotational position for non-indexed connection to the wiring harness.

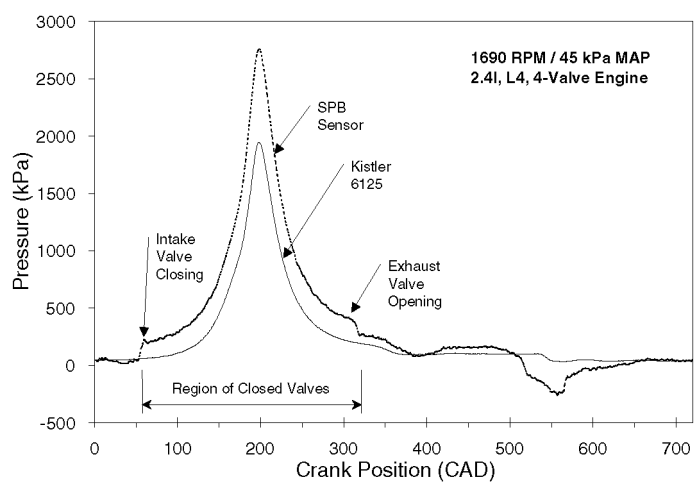


Figure 7. SPB Sensor and Kistler 6125 Signals Plotted as a Function of Crank Position for One Combustion Event at Part Throttle.

Typical sensor signal characteristics for one combustion event are shown in Figure 7 for part-throttle operating conditions. Discontinuities in the sensor waveform are due to intake and exhaust valve loading on the combustion chamber. Differences between the signals during the valves closed region are due to gain and bias differences of the signals. As a measure of sensor linearity, the sensor signal in Figure 7 is plotted as a function of the Kistler 6125 signal (Figure 8). Deviations from the straight line connecting the endpoints of this plot indicate that sensor errors are small relative to the ideal linear response (the primary requirement for PRM).

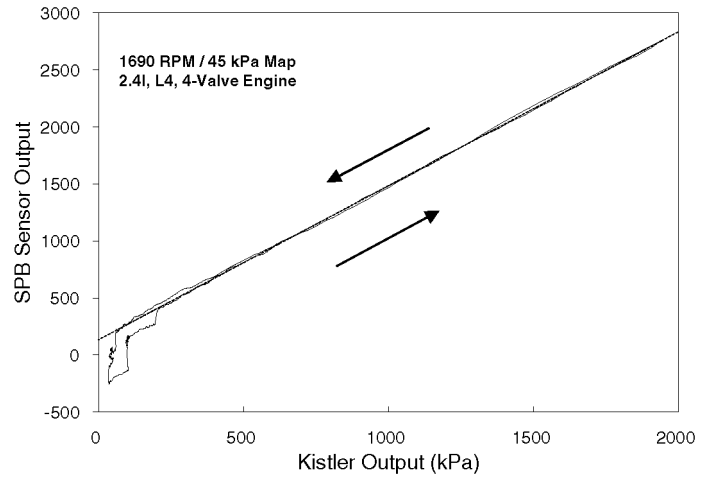


Figure 8. SPB Sensor Signal Plotted as a Function of the Kistler 6125 Signal.

The piezoceramic material used in the sensor is a modified lead-zirconate, lead-titanate composition specially developed for excellent output linearity and stability at high operating temperature. Extensive tests were performed to develop and characterize the electromechanical properties of this material. Results showed that (1) output was insensitive to static preload; (2) non-linearity and hysteresis combined were less than 1.5 percent of full scale over the temperature range; and (3) degradation of charge constant at 13.7 MPa prestress and 150 C was about 2.3 percent per age decade. This material exhibited the most linear response characteristics in tests conducted with materials from leading piezoceramic suppliers worldwide.

To minimize system cost and complexity, and provide high signal quality, a new, high-temperature, integral electronic amplifier was developed. The amplifier circuit schematic is shown in Figure 9. The amplifier utilizes lateral MOSFET transistor technology and Surface Mount Technology (SMT) for high-temperature and high-density circuit packaging. The amplifier operates from a constant-current supply located in the engine control unit (ECU). A single wire connected to the sensor provides power to the amplifier and returns a signal to an electrical interface at the ECU. This enables reduced sensor and connection system costs. The amplifier tolerates contact resistance as high as 10 ohms, which further enables robust, low-cost connection system designs. Figure 10 shows a modular connection system developed as part of this work. The electrical mechanization for the system is shown in the next section.

Measured response characteristics for the electronic system compared to SPICE model predictions are shown in Figures 11 and 12. Linearity is excellent and bandpass characteristics are very stable over the operating temperature range. The amplifier satisfies electromagnetic compatibility (EMC) requirements including electrostatic discharge (ESD) protection and is immune to damage from DC sources. The amplifier, as fabricated on polyimide flexible substrate, has been

tested extensively (thermal shock, thermal cycling, thermal aging) at 150 C without failures.

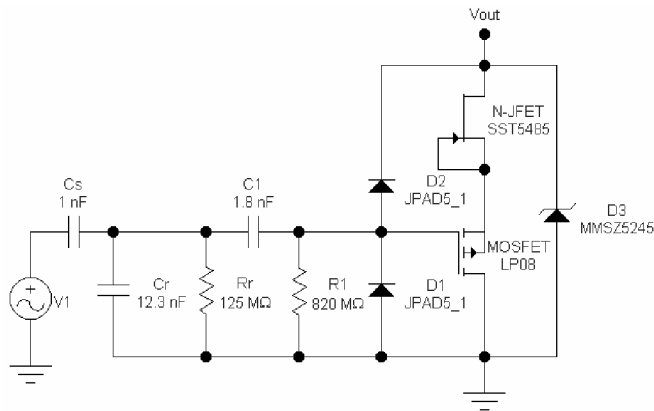


Figure 9. New Integral Electronic Amplifier

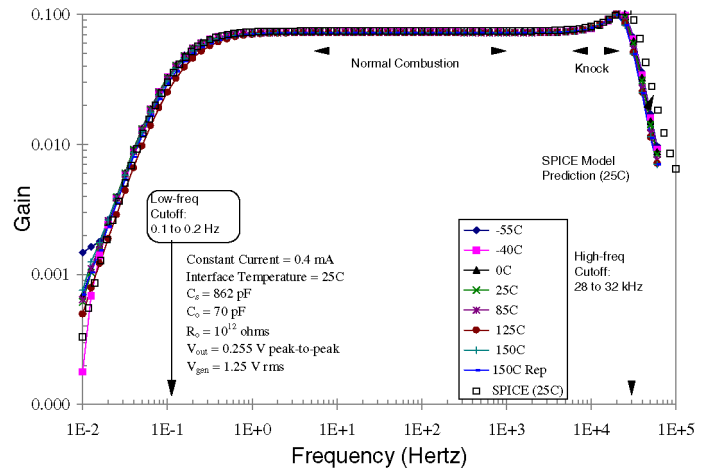


Figure 12. Measured System Bandpass Characteristics Compared to SPICE Predictions.

ENGINE MANAGEMENT SYSTEM

Figure 13 shows an engine management system for a spark-ignited 2.4l four-cylinder engine that uses Pressure-Ratio Management. Each cylinder is equipped with a Spark-Plug-Boss Cylinder Pressure Sensor. The knock sensor, cam sensor, and misfire system, as used conventionally, have been deleted from the system.

The pressure sensor system mechanization showing the system architecture and signal processing paths is shown in Figure 14. The analog interface contains constant current sources to power the pressure sensors. The analog interface also provides some filtering and buffering of the pressure signals. The signals are multiplexed in the pressure acquisition module and sampled by a 10-bit analog-to-digital converter that is clocked by the crank position sensor (encoder). Current production crankshaft position sensors with an accuracy of about +/- 0.25 CAD are sufficient for this system. A Delco GMPX 32U controller was used for system engineering and software development.

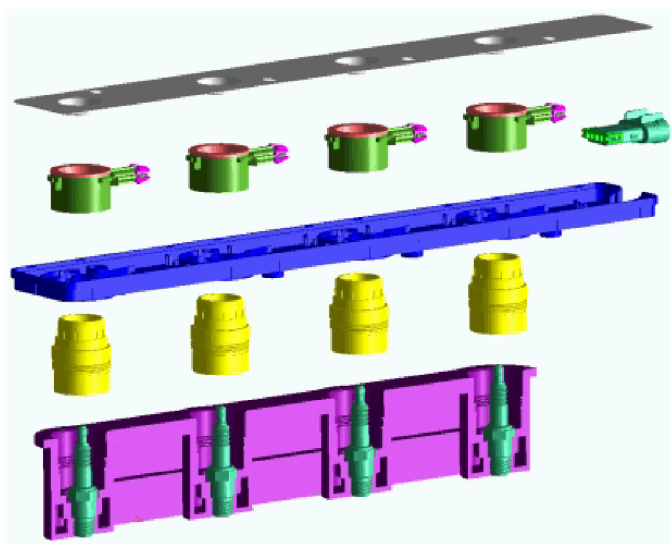


Figure 10. Modular Non-Indexing Connection System Reduces Engine Assembly Costs (exploded view). Design Concept by Delphi Packard Electric Systems.

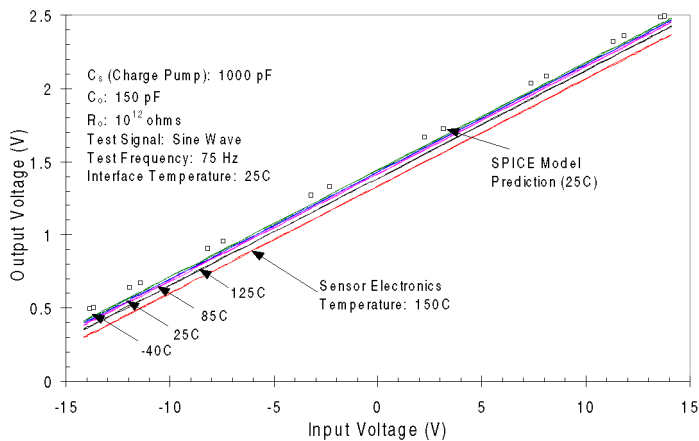


Figure 11. Measured System Linearity Compared to SPICE Prediction for the Temperature Range.

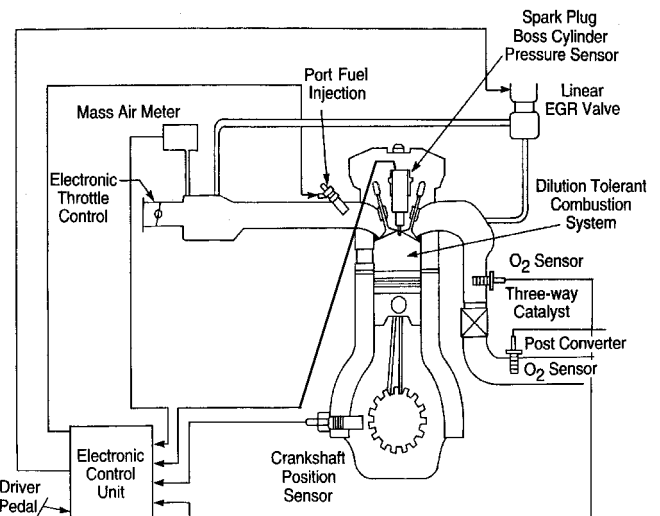


Figure 13. Engine Management System for Spark-Ignited Engine.

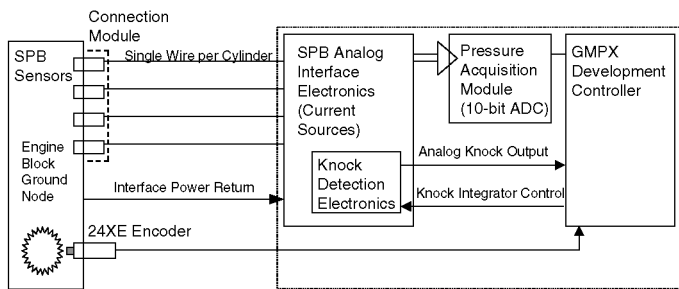


Figure 14. System Mechanization for Pressure Sensor System.

SENSOR SIGNAL ANALYSIS AND VALIDATION

An important step in the development of this pressure-based engine control system was validation of the accuracy of the pressure sensor system per PRM requirements. For this purpose, vehicle tests were conducted on a 2.4l L4 double-over-head-cam (DOHC) engine that was equipped with the system. Pressure sensor errors were measured relative to Kistler 6125 transducers mounted in each cylinder.

Accuracy of the PRM10 Timing Parameter is especially important, since spark timing control and dilution control are based on PRM10 calculations. For 100 consecutive cycles at part-throttle conditions, Figure 15 shows PRM10 calculated from an SPB sensor plotted against PRM10 calculated from the Kistler transducer. Figure 17 compares these data on a cycle-by-cycle basis. The results show that the SPB Sensor provides a good estimate of PRM10. A regression analysis indicates that the PRM10 correlation between the SPB Sensor and the Kistler transducer is excellent.

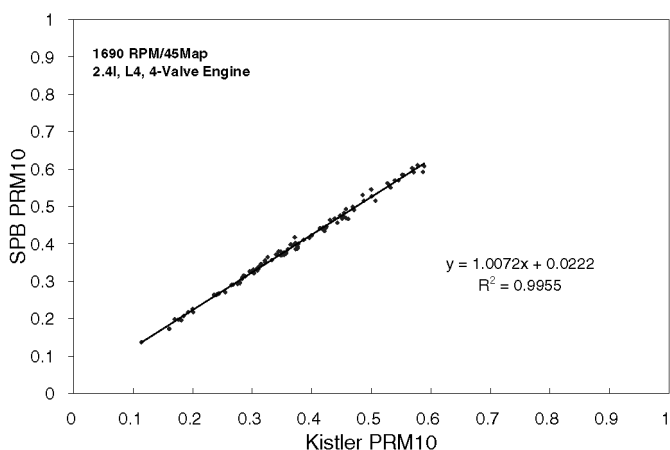


Figure 15. PRM10 Results for SPB Sensor and Kistler for 100 Consecutive Combustion Cycles.

The MPR Dilution Parameter and specifically, variation of MPR are used for Dilution Limit Detection. Figure 16 shows MPR calculated from an SPB sensor plotted against MPR calculated from the Kistler transducer. Figure 18 compares these data on a cycle-by-cycle basis. From the figures, it is apparent that variability of MPR calculated from the SPB Sensor and from the

Kistler is very similar. For this condition, the COV of MPR for the SPB Sensor was 3.2 percent and COV of MPR for the Kistler was 2.9 percent. MPR errors for the SPB Sensor in Figure 16 are a fraction of the MPR fluctuation at this condition, confirming that MPR calculated from the SPB Sensor is appropriate for use for Dilution Limit Detection.

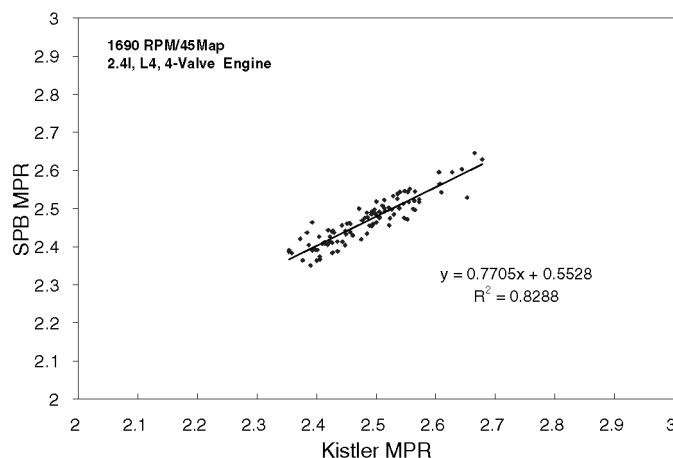


Figure 16. MPR Results for SPB Sensor and Kistler for 100 Consecutive Combustion Cycles.

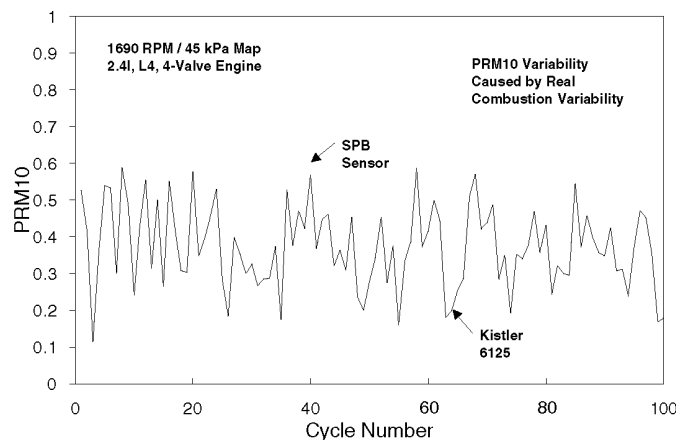


Figure 17. PRM10 vs. Cycle Number for SPB Sensor and Kistler Transducer.

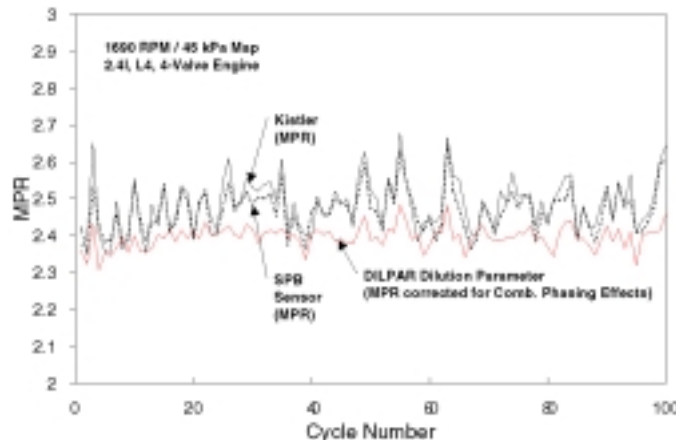


Figure 18. MPR vs. Cycle Number for SPB Sensor and Kistler Transducer.

Figure 18 also shows the dilution parameter, DILPAR for these data. DILPAR is basically MPR that is corrected for combustion phasing effects (see equation 5). Figure 18 shows that DILPAR is relatively invariant for this steady state operating condition. This means that DILPAR can essentially provide a one-cycle estimate of combustion dilution. The observed variability of DILPAR in Figure 18 is attributed to system noise and real A/F variations caused by fuel control based on an exhaust oxygen sensor.

Additional tests were performed to measure the accuracy of the SPB Sensor System for the range of engine operating conditions encountered in the FTP test. "Maximum errors" for PRM10 and MPR as measured for 100 consecutive cycles are reported as shown in Figures 19 and 20. Average errors for these conditions are much less. Correlation coefficients are also shown. These results establish the validity of the SPB Sensor system for use with Pressure-Ratio-Management.

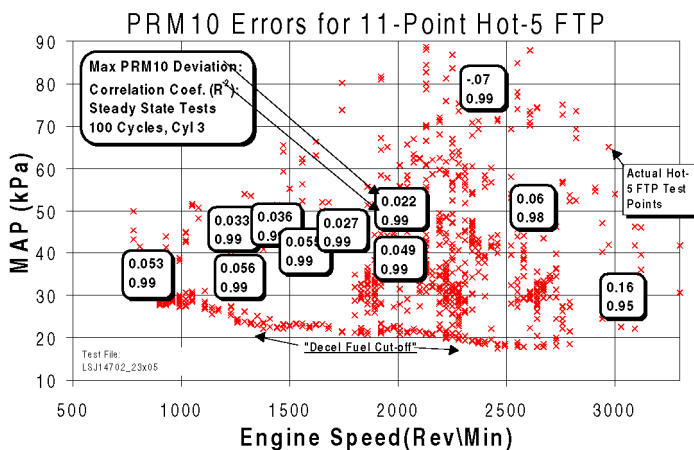


Figure 19. PRM10 Errors for Simulated FTP Test.

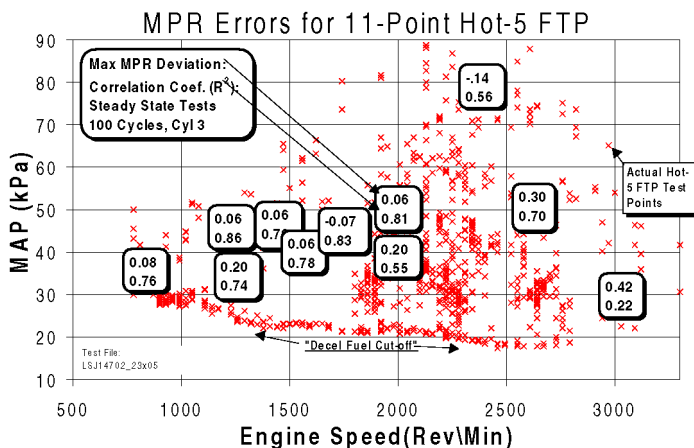


Figure 20. MPR Errors for Simulated FTP Test.

ENGINE CONTROL APPLICATIONS

CLOSED-LOOP SPARK TIMING AND EGR CONTROL – Conventional open-loop engine control systems are inherently unable to compensate for manufacturing variations, aging and wear, fuel properties, and some environmental factors like humidity [49].

Because of this, and in order to maintain acceptable driveability, open-loop systems must be calibrated with lower levels of EGR than the engine can tolerate. Even for moderate levels of EGR, engine operation may be compromised by misdelivery of EGR and improper spark timing for the mixture delivered. Closed-loop control using cylinder pressure measurements provides precise regulation of spark timing and EGR, resulting in optimum engine efficiency and minimum emissions.

Closed-loop, MBT, spark-timing control was implemented by controlling PRM10 to a nominal target value of 0.55. Modifications to the PRM10 target were made for special operating conditions and were input as calibration parameters in a lookup table. For decels, PRM10 target values were reduced to maintain good combustion stability. PRM10 target values were also automatically modified if knock was detected or if pre-ignition was detected. PRM10 target values may also be reduced to reduce NOx emissions although with an associated efficiency loss.

Closed-loop EGR control was implemented using Method 2, Dilution Control. Spark advance targets for the best efficiency mixtures were determined in off-line experiments and were input into a look-up table. Method 3, Dilution Limit Detection, was used simultaneously to limit EGR rates if combustion instabilities or partial-burn cycles were detected. For good transient control of EGR, additional improvements were incorporated including 1) accurate EGR lift control with improved valve stability, 2) use of an EGR transport delay model, and 3) adaptive learning for the EGR valve lift table.

Figures 21 and 22 show HC emissions, NOx emissions, and fuel efficiency as a function of the PRM10 target value at 1800 rpm and part throttle. Figure 21 is for EGR disabled with a corresponding MBT spark advance of 30 CAD BTDC. Figure 22 is for heavy EGR corresponding to the best efficiency mixture and an MBT spark advance of 52 CAD BTDC. The data shows that control of PRM10 to a target value of 0.55 does provide the best efficiency operation for conditions with and without EGR. Heavy EGR, corresponding to the best efficiency mixture, improved engine efficiency by 5 percent and reduced engine-out NOx emissions about 70 percent. Engine-out HC emissions were increased about 40 percent. For systems without EGR or for systems with moderate EGR, spark retard is normally used to suppress engine-out NOx. This may reduce efficiency an additional 2 to 3 percent relative to operation with the best efficiency mixture and MBT spark timing.

Federal Test Procedure (FTP) tests were performed to evaluate the performance of the engine and control system for urban driving. These results establish that high levels of EGR can be used to improve fuel economy. For any vehicle application, the net benefit of EGR on fuel economy depends on transmission characteristics and power-to-weight ratio of the engine and vehicle.

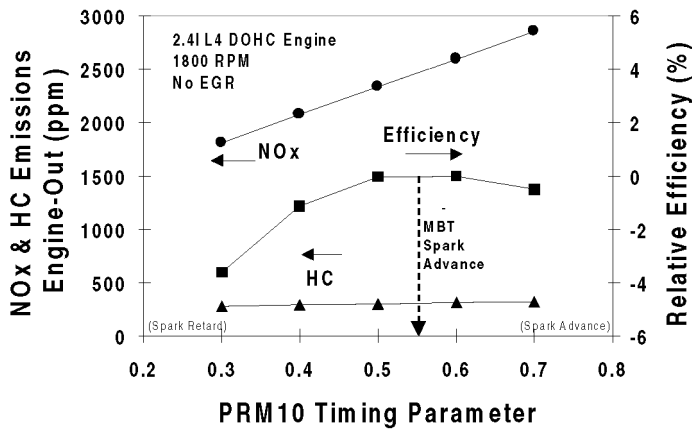


Figure 21. Fuel Economy and Emissions as a Function of the PRM10 Timing Parameter for Operation without EGR.

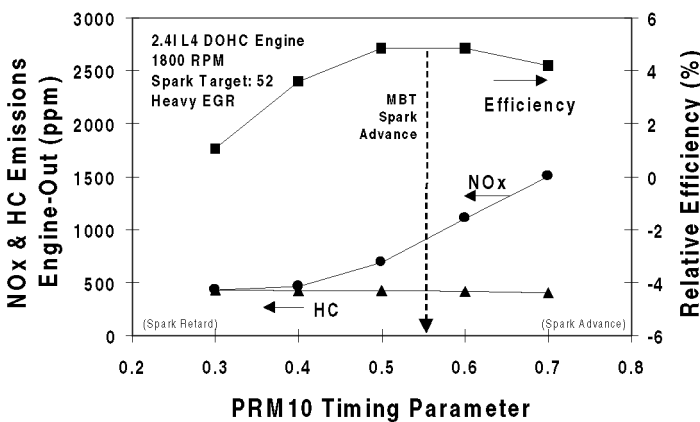


Figure 22. Fuel Economy and Emissions as a Function of the PRM10 Timing Parameter for Operation with Heavy EGR.

AIR-FUEL RATIO BALANCING – Cylinder-to-cylinder A/F imbalances in spark-ignited engines may originate from both unequal fuel flow and unequal airflow to the cylinders. Typically, production injectors have matched flow rate within 3 to 6 percent. Over life as injectors age, fuel delivery may be altered by an additional + / - 10 percent. The combined effect can be substantial, and may approach a four A/F spread. A/F imbalances can also result from fuel transport among cylinders caused by strong intake back flows at light-load operating conditions.

A/F imbalances can significantly compromise engine operation and control in a variety of ways. Driveability problems can arise because of reduced dilution tolerance for cylinders with leaner mixtures. This may limit maximum calibrated EGR levels. Air-fuel control accuracy may also be compromised and may result in both increased emissions and increased variation of emissions vehicle-to-vehicle. Generally, engine performance will be reduced by A/F imbalances since one or more cylinders may not be fueled optimally for maximum power generation.

Cylinder pressure-based control can improve engine operation by correcting for A/F imbalances cylinder-to-cylinder. The method for balancing A/F among cylinders assumes that combustion burn rate differences among cylinders are caused by A/F differences alone. The algorithm implemented is based on Method 2, Dilution Control applied to dilution with excess air as described on page 5.

To illustrate the basis for the algorithm, Figure 23 shows a plot of MBT spark advance as a function of A/F ratio. Leaner mixtures require more spark advance and richer mixtures require less. Typical sensitivity is five CAD spark advance per air-fuel ratio. The data in Figure 24 shows that this is valid for A/F ratios as rich as 13.0.

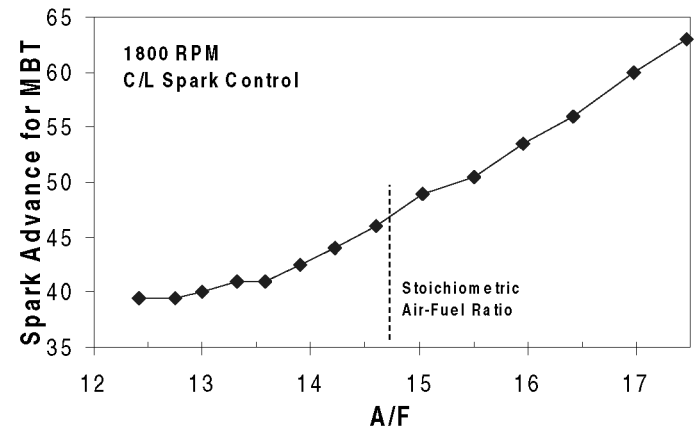


Figure 23. Spark Advance at MBT as a Function of Mixture A/F.

The A/F Balancing algorithm operates simultaneously with closed-loop (C/L) spark-timing control using PRM10. First, spark timing for each cylinder is adjusted to MBT. Then, the A/F balancing algorithm compares each cylinder's spark advance to the average and increments the individual-cylinder fueling multipliers up or down while maintaining constant total fuel delivery. More fuel is delivered to the lean cylinders and less to the rich. The balancing algorithm operates in a significantly slower loop than the spark timing and EGR control loops. Based on sensor repeatability cylinder-to-cylinder of about PRM10 +/- 0.025, the expected accuracy of the A/F balancing algorithm is +/- 0.25 A/F ratio or +/- 1.5 percent.

The performance of the A/F balancing algorithm was tested by running Hot-5 FTP tests. During the tests, the air-fuel ratio was controlled using the production exhaust oxygen sensor and A/F-control algorithms. The exhaust A/F ratio was measured using an NGK A/F sensor. As shown in Figure 24, when one cylinder was artificially biased 10 percent lean, the overall exhaust A/F was biased lean and tailpipe NOx emissions increased. When the A/F balancing algorithm was invoked, the enleaned cylinder could be detected and corrected for. A similar effect was observed when one cylinder was artificially biased 10 percent rich, as shown in Figure 25. The overall exhaust A/F was biased rich and this increased tailpipe HC emissions significantly.

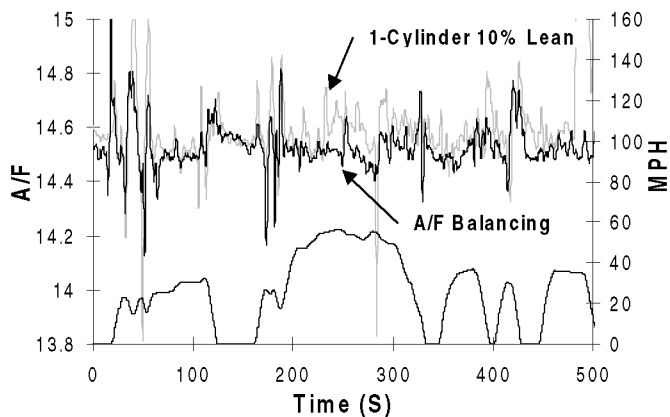


Figure 24. Measured A/F Ratio for Hot-5 FTP Test for A/F Balancing and for One Cylinder Biased 10 Percent Lean.

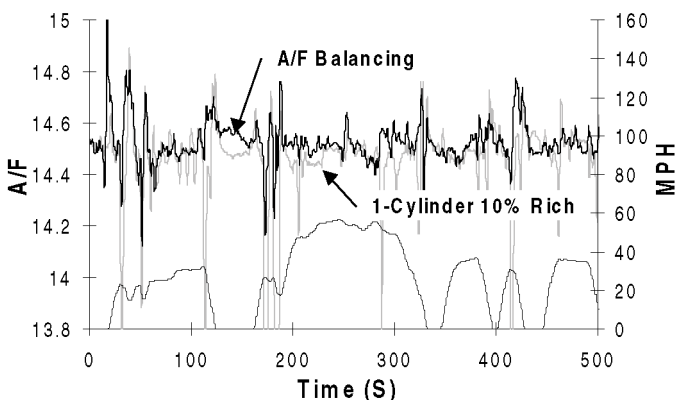


Figure 25. Measured A/F Ratio for Hot-5 FTP Test for A/F Balancing and for One Cylinder Biased 10 Percent Rich.

The basic method presented is based on the assumption that A/F ratio alone is responsible for burn-rate differences among cylinders. Other causes of burn rate differences include EGR maldistribution or variations of in-cylinder flow patterns. For engines with these problems, performance of the A/F Balancing algorithm may be effected. EGR maldistribution and variations of in-cylinder flow patterns are usually a function of geometry and may be repeatable from vehicle to vehicle. A primary calibration with balanced injectors could provide a reference from which a rebalance of injectors would be possible. Alternately, EGR could be disabled periodically in the field, and injector and airflow imbalances could be corrected.

MISFIRE AND PARTIAL-BURN DETECTION – The objective of the misfire detection system is to satisfy OBD II requirements for catalyst protection over the full range of engine operating speed and load. A misfire detection system has been implemented using MPR since MPR is fundamentally a direct indicator of the heat release per unit charge mass [70]. The method is also applicable to the detection of partial-burn cycles. The overall method is summarized in the table below. Required accuracy of MPR is nominally ± 0.3 .

Calculated MPR Value	Diagnostic Result
$2 < \text{MPR} < 3.5$	Normal Complete-Burn Cycles
$\text{MPR} \sim 0$	Total Misfire Cycles
$0 < \text{MPR} < 2$	Partial-Burn Cycles

The strategy is illustrated in Figure 26 which shows test results from an engine in which the A/F was varied from stoichiometric to very lean. This produced combustion cycles that were retarded and generally incomplete. The figure shows MPR plotted against IMEP for 200 consecutive cycles as measured using a Kistler pressure transducer. There is good correlation between MPR and IMEP, which shows that MPR is a good estimator of indicated work per cycle.

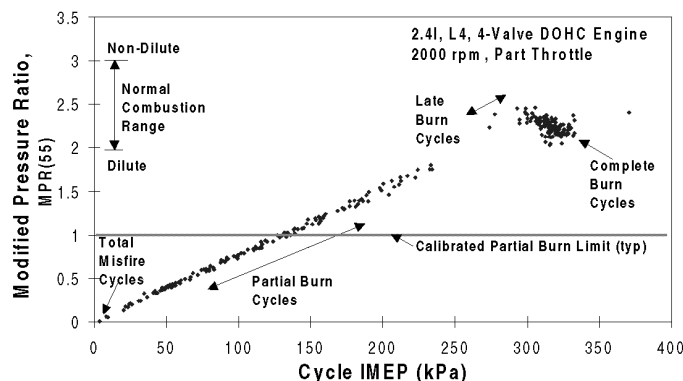


Figure 26. MPR(55) vs. IMEP for Kistler Pressure Transducer.

For normal combustion conditions, heat release is complete before the 55 CAD ATDC sample point. For abnormal combustion cycles with very late burn characteristics, the potential exists for cycles that have not necessarily completed burning by 55 CAD ATDC. To determine if burning occurs beyond 55 CAD ATDC for late-burn and partial-burn cycles, both MPR at 55 ATDC and MPR at 120 ATDC were calculated. The 120 CAD ATDC sample point corresponds to a crank position just before the exhaust valve opens.

Figure 27 shows a plot of MPR(120) vs. MPR(55). The lower dashed line corresponds to equal pressure ratios for both sample points. For cycles along this line, burning has ceased by 55 CAD ATDC. For cycles along or near the upper horizontal line, combustion was complete by 120 CAD ATDC ($1.8 < \text{MPR}(55) < 2.0$). For cycles with MPR(55) between 0.5 and 1.8, combustion was incomplete. Most cycles had late burning. For cycles with MPR(55) below about 0.5, no more than 25 percent of the charge has burned and combustion was quenched.

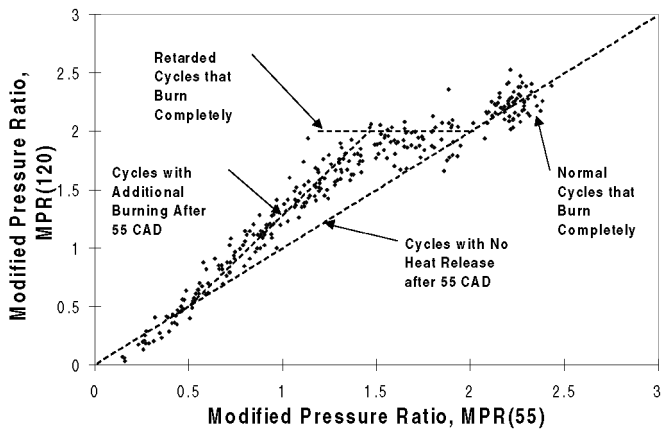


Figure 27. MPR(120) vs. MPR(55) for Kistler Pressure Transducer.

The data in Figure 27 shows that if any heat release occurs after 55 CAD ATDC, its contribution to MPR is at most about 25 percent and virtually no useful work was done (see IMEP in Figure 26). It is concluded that MPR(55) is an appropriate parameter for misfire detection.

If more detailed heat release information is needed, an additional pressure sample at 100 or 115 CAD ATDC could be obtained. MPR(55) (or say MPR(115)) is useful for monitoring the extent of combustion for the cold start. To promote catalyst heating during the cold start, spark timing is retarded heavily and this can lead to partial burning for some cycles. MPR(55) can be used to insure that spark timing is not retarded excessively and combustion is complete within the cylinder before exhaust valve opening and quenching occurs.

Tests were performed using this misfire algorithm with the Spark-Plug-Boss Sensor System over a wide range of engine speeds at “zero brake torque” (neutral gear) to simulate worst case conditions. The mixture was enleaned to create a distribution of total misfire, partial-burn, and complete-burn cycles. One hundred consecutive cycles were sampled at each speed. A Kistler pressure transducer mounted in each cylinder was used as a reference.

Figures 28 through 31 show MPR(55) plotted vs. IMEP for 1250, 2000, 3000, and 4000 rpm, respectively. The data shows that partial burn cycles and total misfire cycles were easily detected by the system. Cycles with an MPR of about 1.8 to 2.0 correspond to “complete burn” cycles with an indicated mean effective pressure (IMEP) of 200 to 300 kPa. Cycles with an MPR of zero and IMEP of zero (or slightly negative), correspond to “total misfires”.

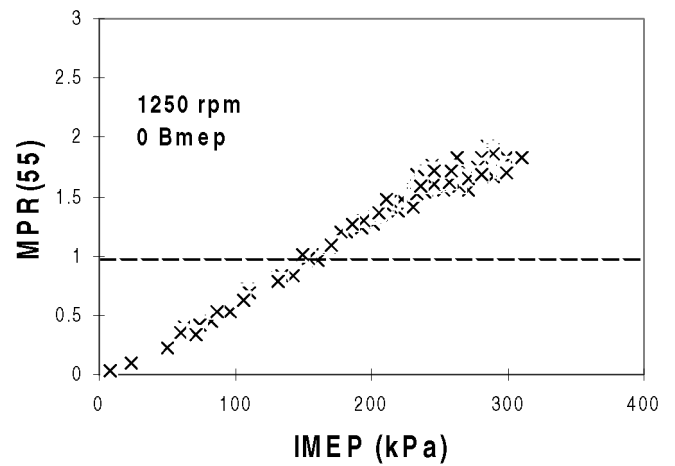


Figure 28. MPR vs. IMEP at 1250 rpm and Zero Brake Torque.

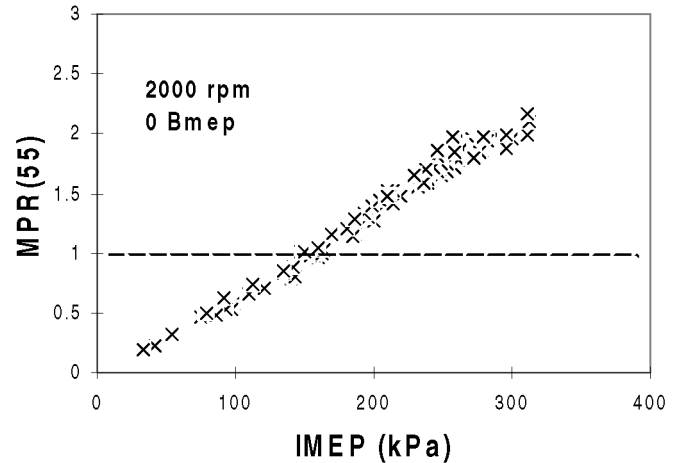


Figure 29. MPR vs. IMEP at 2000 rpm and Zero Brake Torque.

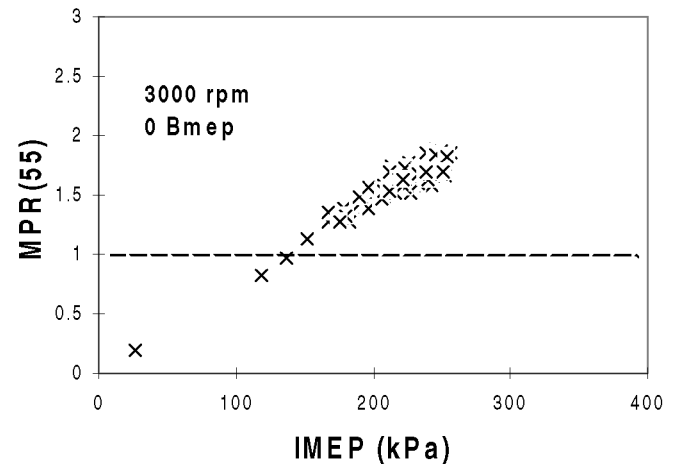


Figure 30. MPR vs. IMEP at 3000 rpm and Zero Brake Torque.

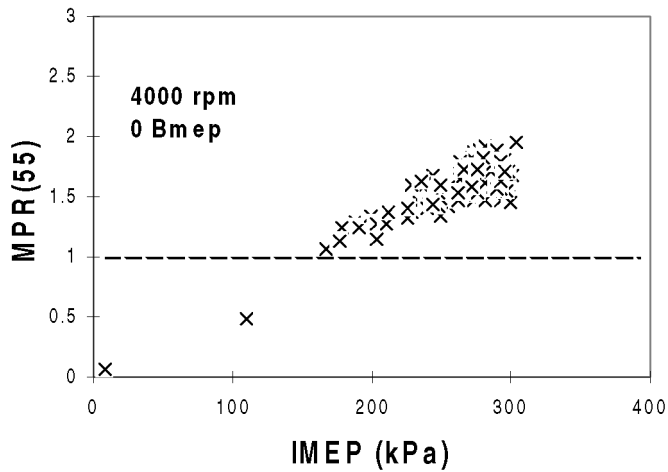


Figure 31. MPR vs. IMEP at 4000 rpm and Zero Brake Torque.

Depending on OBDII requirements and system requirements for misfire detection, the system may be calibrated to simply detect total misfires or may be calibrated more aggressively to detect partial-burn cycles. Partial-burn cycles may also contribute to catalyst degradation. An MPR of 1.0 was chosen as an example of a partial-burn threshold in figures 28 through 31.

COLD START CONTROL – The “cold start” is a critical portion of the FTP test and is responsible for the majority of HC emissions generated for this test. In order to tolerate the incomplete evaporation of fuel with acceptable driveability, open-loop fueling calibrations for the cold start must be biased rich. This typically results in a 40 to 50 percent HC emissions penalty relative to a cold start with ideal fuel delivery. Open-loop spark timing control is also used during the cold start. Since the gas-phase A/F and combustion burn rates depend on the completeness of fuel evaporation, spark timing must be advanced to prevent partial burn cycles. This increases the catalyst light-off period and further increases HC emissions. Even with optimized spark and fueling calibrations for the cold start, many production vehicles suffer from poor driveability when the lowest volatility fuels are used.

Cylinder pressure sensing and Pressure-Ratio Management can improve engine control during the cold start in several ways:

1. Method 2 Dilution Control (see page 5) can be used to control the gas-phase A/F slightly lean of stoichiometric. This prevents over fueling and reduces HC emissions.
2. Closed-loop (C/L) spark-timing control using PRM10 and PRM25 can provide precise “spark retard control” and improve catalyst heating.
3. Spark retard is needed for catalyst heating but excessive retard will increase HC emissions due to incomplete combustion. MPR measured during the expansion stroke can be used to indicate

- completeness of combustion before exhaust valve opening to insure that spark retard is not excessive.
4. Cylinder pressure-based control can also simplify and speed the tedious cold-start calibration process.

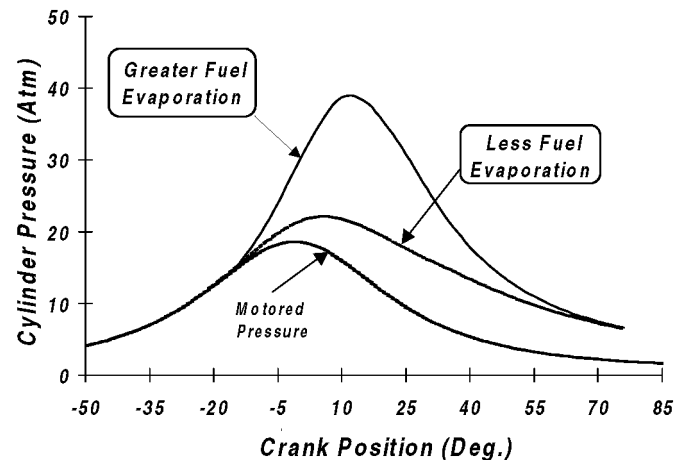


Figure 32. Typical Cylinder Pressure Waveforms for the Cold Start with Greater and Less Fuel Evaporation.

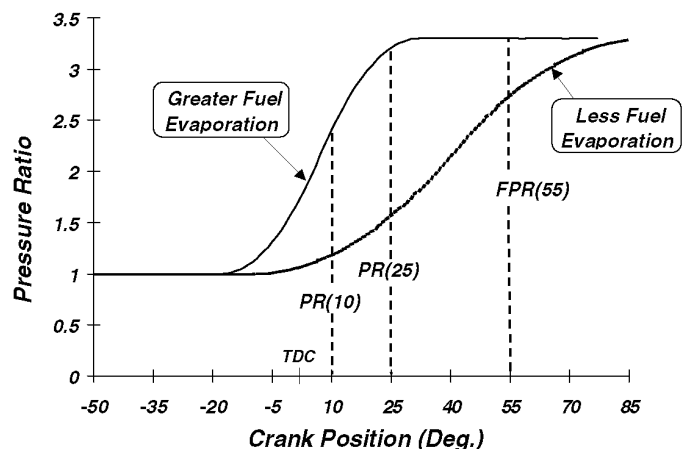


Figure 33. Typical Pressure-Ratio Waveforms for the Cold Start with Greater and Less Fuel Evaporation.

To demonstrate the basis for A/F control during the cold start, Figures 32 and 33 show typical cylinder pressure waveforms and calculated pressure ratios, respectively, for combustion with greater fuel evaporation and combustion with less fuel evaporation. For fixed spark timing, reduced burn rate for combustion with less fuel evaporation causes a significantly later burn with incomplete heat release by the 55 CAD ATDC sample point. This produces reduced PRM10 (and PRM25) and reduced FPR (MPR) as shown in Figure 33.

KNOCK DETECTION – The Spark-Plug-Boss Sensor is located a short distance directly above each combustion chamber. The mechanical load path between the combustion chamber and the sensor is very stiff and provides good response to knock-induced structural vibrations over a wide range of frequencies. Valve train noise, such as noise created at valve closing, occurs

outside the knock interval and may be windowed out using available signal processing techniques. Since the SPB Sensor is located relatively far from the engine block, sensitivity to block noise is generally low.

Figures 34, 35, and 36 show measured knock frequency spectra for the SPB Sensor, a flush-mounted 6125 Kistler transducer, and a flat response knock sensor, respectively, at 1200 rpm. Spectra were obtained for multiple windowed knocking cycles for light knock (0.25 to 0.5 bar, peak-to-peak), medium knock (0.75 to 1 bar, peak-to-peak), heavy knock (2.7 to 3.3 bars, peak-to-peak), and no knock.

The spectra indicate that the dominant first circumferential mode is clearly detected by the SPB Sensor, the Kistler, and the knock sensor. This shows that the SPB Sensor is sensitive to the first mode of knock even though a node of acoustic resonance for this mode exists on the chamber centerline. For heavy knock, the Kistler spectra indicates a strong mode at about 10 kHz, but this mode was only weakly detected by the SPB Sensor and the knock sensor. The Kistler spectra also indicate a weaker mode at 12 to 13 kHz, which may be the first radial mode of knock. The SPB Sensor and the knock sensor also detect this weaker mode. Interestingly, the SPB Sensor uniquely reveals a strong mode at about 18 kHz. This may be an axial mode of knock theoretically centered at 18 to 19 kHz. The spectral width is quite wide, as desired, and may be due to the dependence of resonant frequency on piston position. High-frequency knock modes are generally desirable for knock detection because of their potentially high signal-to-noise ratios.

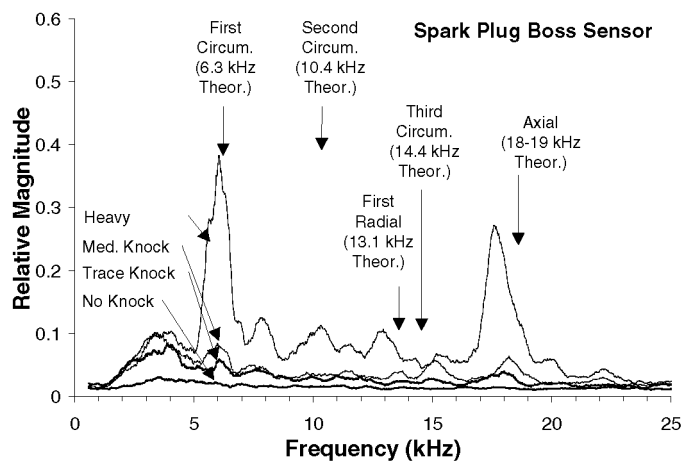


Figure 34. Knock Frequency Spectra for SPB Sensor at 1200 rpm for Light, Medium, Heavy, and No Knock.

To evaluate the ability of the SPB Sensor to detect knock in a system, tests were conducted on an engine dynamometer using flush-mounted 6125 Kistler transducers and the production knock sensor as references. Signals for 200 consecutive cycles were bandpass filtered with an 8-pole Butterworth filter from 5

to 25 kHz (all modes of knock) and windowed from 0 and 90 CAD ATDC. The integrated result over this window was recorded as knock intensity.

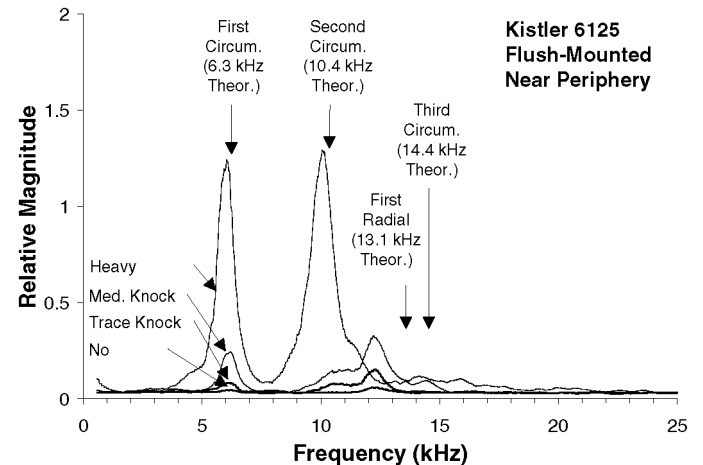


Figure 35. Knock Frequency Spectra for Flush-Mounted Kistler 6125 Transducer at 1200 rpm for Light, Medium, Heavy, and No Knock.

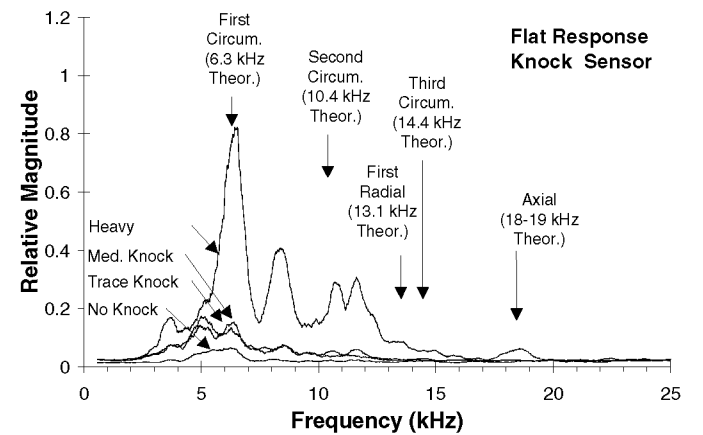


Figure 36. Knock Frequency Spectra for Flat-Response Knock Sensor at 1200 rpm for Light, Medium, Heavy, and No Knock.

Typical results are shown in Figures 37 and 38 for engine tests at 2000 rpm, 95 MAP, and A/F of 14.6. Figure 37 shows knock intensity for the SPB Sensor plotted against knock intensity for the Kistler transducer. The correlation coefficient, based on a regression analysis for this data, was 0.76. This is significantly better than the correlation coefficient for the knock sensor, which was only 0.32 (Figure 38). Improvement in knock detection for the SPB Sensor is most evident at low levels of knock intensity where the sensors background noise is very low (see Figure 37). This is important to insure good detection of trace knock without “false knock retard”. By comparison, the knock sensor has relatively high background noise levels as shown in Figure 38. Further improvements in knock detection using SPB Sensors may be possible with a dual mode detector using the first circumferential mode and the 18 kHz signal shown in Figure 34.

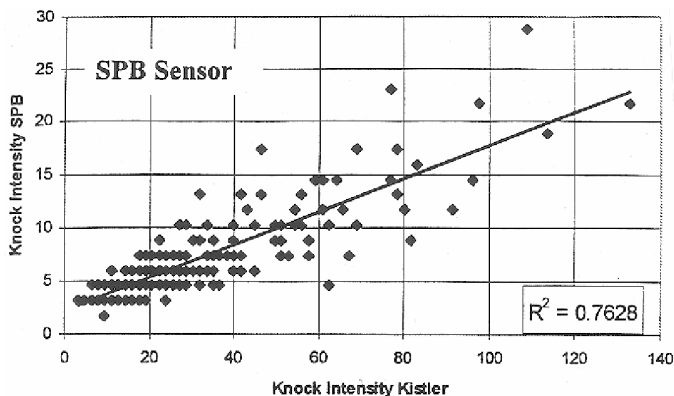


Figure 37. 77Knock Intensity for the SPB Sensor vs. Knock Intensity for a Flush-Mounted Kistler Transducer at 2000 rpm and 95 MAP.

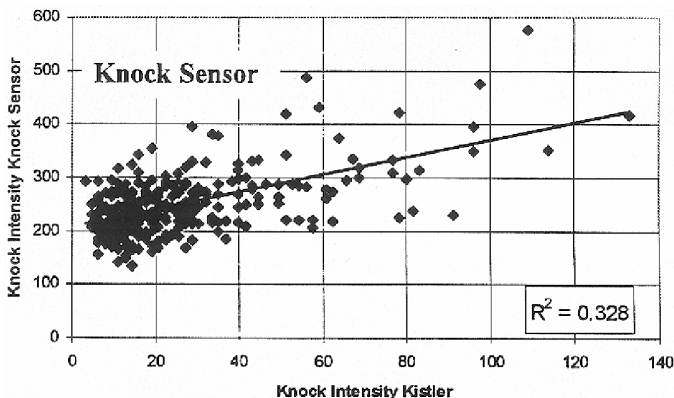


Figure 38. Knock Intensity for the Knock Sensor vs. Knock Intensity for a Flush-Mounted Kistler Transducer at 2000 rpm and 95 MAP.

SUMMARY AND CONCLUSIONS

A production-viable cylinder-pressure-based engine control system with extensive system benefits has been demonstrated on a spark-ignited four-cylinder gasoline engine. The system adaptively optimizes combustion for every cycle in each cylinder over the life of each vehicle. Precise engine control was demonstrated for a variety of functions including spark timing control, dilution control, A/F balancing, cold start fueling, misfire detection, and knock detection.

The current work offers a new solution to the technical and commercial limitations of other pressure-based control systems. The technology developed reduces the cost and complexity historically associated with pressure-based systems, while providing increased control functionality. An essential objective of the work was to develop robust, computationally efficient algorithms that do not require highly accurate or absolute measures of cylinder pressure. Pressure-Ratio-Management was presented and the ratio of fired-to-motored pressure was established as a means to efficiently estimate combustion phasing and mixture dilution for each cycle.

A non-intrusive cylinder pressure sensor that satisfies PRM requirements was conceived and developed. The sensor uses piezoelectric sensing technology to detect compressive forces in the spark plug boss of four-valve-per-cylinder engines in response to cylinder pressure. The sensor incorporates a linear piezoceramic material and a high-temperature integral electronic amplifier. A single wire connected to the sensor provides a constant current to the amplifier and returns a voltage signal to an electrical interface at the engine controller. The sensor system has potentially excellent durability with estimated cost between one half to one quarter that of competitive intrusive sensors.

The control system has potential to measure trapped air in each cylinder using cylinder pressure measurements. Possibly, the air meter may be eliminated and system cost further reduced. Additional work is needed to develop this functionality. Although the system has been applied to conventional S.I. engines in this work, extension to the common-rail diesel, direct-injection gasoline, and homogeneous-charge compression ignition engines may enable combustion control for these engines as well.

ACKNOWLEDGEMENTS

The authors gratefully acknowledge the engineers and technicians who contributed to the success of this work. Those persons are: Mr. Robert Bartley at Delphi-Packard, Mr. Robert Bayer at GM R&D, Mr. Edward Bungo at Delphi-Packard, Mr. Marvin Carpenter at GM R&D, Mr. Anthony Corso at Delphi-Packard, Mr. Michael L. Crenshaw at GM R&D, Mr. Robert He at GM R&D, Mr. Louis Jerzy at GM R&D, Dr. Scott W. Jorgensen at GM R&D, Dr. John Kirwan at Delphi-Energy, Mr. Tom Livingstone at GM R&D, Mr. Tom Robertson at GM R&D, Dr. James F. Sinnamon at Delphi R&D, Dr. Gerald Szekely at GM R&D, Mr. Brian Thompson at GM Powertrain, Mr. Ray Tidrow at GM R&D, Mr. Robert Vitale at GM Mid-Lux, and Mr. Andy Voss, Mr. Gene Ripley, and Mr. Eric Norppa at Delphi Delco Electronics Systems.

REFERENCES

1. Amann, C., "Cylinder-Pressure Measurement and Its Use in Engine Research", SAE Paper 852067, 1985.
2. Powell, B.K., Lawson, G.P., and Hough, G., "Advanced Real Time Powertrain System Analysis", ASME Journal, #87-ICE-46.
3. Tuscott, A., et al., "The Application and Evaluation of a Novel Engine Management System Based on Intelligent Control and Diagnostics Algorithms and Utilizing Innovative Sensor Technology", presented at the Advanced Microsystems for Automotive Applications 99 Conference, Germany, March, 1999.
4. Wibberley, P., and Clark, C., "An Investigation of Cylinder Pressure as Feedback for Control of Internal Combustion Engines," SAE Paper 890396, 1989.

5. Pestana, G., "Engine Control Methods Using Combustion Pressure Feedback," SAE Paper 890758, 1989.
6. Hata, Y., and Asano, M., "New Trends in Electronic Engine Control: To the New Stage," SAE Paper 860592, 1986.
7. Kusakabe, H. et al, "A Cylinder Pressure Sensor for Internal Combustion Engine," SAE Paper 920701, 1992.
8. Winter, H., Mock, R., and Meixner, H., "A High Temperature Pressure Sensor for the Combustion Chamber of Spark Ignition Engines," 18th International Symposium Automotive Technology 1988, Vol. 2, 88103.1, 1988.
9. Mock, R., and Meixner, H., "A Miniaturized High-Temperature Sensor for the Combustion Chamber of a Spark Ignited Engine," Sensors and Actuators A, 25-27 (1991) 103-106.
10. Nobuyoshi, S., et al, "Combustion Pressure Sensor for Toyota Lean Burn Engine," SAE Paper 930882, 1993.
11. Takeuchi, M., et al, "A Combustion Pressure Sensor Utilizing Silicon Piezoresistive Effect," SAE Paper 930351, 1993.
12. Ueda, M., et al, "Combustion Pressure Sensor for Toyota Lean Burn Engine Control – Engine Cylinder Pressure Sensor with Piezoresistive Silicon Device," JSAE 924126, 1992.
13. Akita, T., "Technology of Laser Welding for the Diaphragm of Combustion Pressure Sensor – Analysis of Transient Response of Sensing Element During Welding," JSAE 924127, 1992.
14. Anastasia, C. and Pestana, G., "A Cylinder Pressure Sensor for Closed Loop Engine Control," SAE Paper 870288.
15. Howng, W., "Cylinder Pressure Transmitter for an Internal Combustion Engine," US Patent, 4,620,438, Nov. 4, 1986.
16. Lukasiewicz et al, "Cylinder Pressure Sensor for an Internal Combustion Engine," US Patent 5,038,069, Aug. 6, 1991.
17. Lukasiewicz et al, "Cylinder Pressure Sensor for an Internal Combustion Engine," US Patent 5,126,617, Jun. 30, 1992.
18. Herden, W., and Kusell, M., "A New Combustion Pressure Sensor for Advanced Engine Management," SAE Paper 940379, 1994.
19. Kusell, M., "Dimensionierung eines Brennraumdrucksensors für Regelungsaufgaben in Serienmotoren", Phd. Dissertation, Technical University of Carolo-Wilhelmina, January 26, 1994.
20. Taylor, H., et al, "Fiber Optic Pressure Sensors for Internal Combustion Engines," Applied Optics, 1993.
21. Mobley, C., "Non-Intrusive In-Cylinder Pressure Measurement of Internal Combustion Engines," SAE Paper 1999-01-0544, 1999.
22. Miyamoto, N., et al, "Unique Measuring Method of Indicator Diagrams Using Strain History of Headbolts," SAE Paper 800983, 1980.
23. Brandt, H., and Gibson, F., "Dynamic Combustion Characteristic Sensor for Internal Combustion Engine," US Patent 4,491,010, Jan. 1, 1985.
24. Cobb, D., "Gasket with Encased Load Sensor," US Patent 5,121,929, Jun. 16, 1992.
25. Yoshiki, C., et al, "Device for Detecting Combustion Pressure of an Internal Combustion Engine," European Patent Application 91114200.8, Feb. 26, 1992.
26. Takeuchi, K. "Cylinder Pressure Measurement Using a Spark-Plug Pressure Sensor," JSAE Review Volume 11, No. 3 (July1990).
27. Frelund, A., "Engine Combustion Chamber Pressure Sensor," US Patent 4,601,196, Jul.22, 1986.
28. Pozniak, D., "Peak Combustion Pressure Timing Detector for IC Engine Using Intake Valve Deformation," US Patent 4,672,843, Jun. 16, 1987.
29. Kleinschmidt, P., and Magori, V., "Pressure Sensor for an Internal Combustion Engine," US Patent 4,382,377, May 10, 1983.
30. Taylor, H., et al, "Metal-Embedded Fiber-Optic Fabry-Perot Sensors," Optical Society of America, Vol. 16, No. 24, Dec. 1991.
31. Randall, K., and Powell, D., "A Cylinder Pressure Sensor for Spark Advance Control and Knock Detection," SAE Paper 790139.
32. Kondo, M. "Indiscope – A New Combustion Pressure Indicator with Washer Transducers," SAE Paper 750883, 1975.
33. Vickers, D., and Wlodarczyk, M., "A Fiber Optic Sensor for Combustion Pressure Measurement in a Washer Configuration," Proc. SPIE, Vol. 840, 1987.
34. Sawamoto, K., et al., "A Newly-Developed Cylinder Pressure Sensor as Part of an Individual Cylinder Knocking Control System," IECON'86, 1986.
35. Sawamoto, K., et al., "Individual Cylinder Knock Control by Detecting Cylinder Pressure," SAE Paper 871911, 1987.
36. Meyer, R.C., "Spark Plug/Pressure Sensor Device," US Patent 5,672,812, Sept 30, 1997.
37. Morris, J., and Li-Chi, "Improved Intra-Cylinder Combustion Pressure Sensor," SAE 850374, 1985.
38. Morris, J., "Intra-Cylinder Combustion Pressure Sensing," SAE Paper 870816, 1986.
39. Wlodarczyk, M., et al, "Low-Cost Spark Plug-Integrated Fiber Optic Sensor for Combustion Pressure Monitoring," SAE Paper 930853, 1993.
40. Wlodarczyk, M., et al, "High Temperature Performance Analysis of Automotive Combustion Pressure Sensor," Proc. of SPIE, Vol. 1799, 1992.
41. Wlodarczyk, M., et al, "Fiber Optic Pressure Sensor for Combustion Pressure Monitoring and Control," Proc. SPIE, Vol. 1587, 1991.
42. Sasayama, T., et al, "An Advanced Engine Control System Using Combustion Pressure Sensors," IECON'85, Volume I, pg 68,1985.
43. Hazelden, R., et al, "Fiber Optic Pressure Sensor for Internal Combustion Engines," SPIE Vol. 1040, 1988.

44. Fuji, I., "MBT Control Utilizing Crank Angle of Maximum Combustion Pressure," SAE Paper 890759, 1989.
45. Yagi, S., et al., "MBT Control Utilizing Crank Angle of Maximum Combustion Pressure," Honda R&D Technical Review, Vol. 2, 1990.
46. Hata, Y., et al., "Engine Control System Using Cylinder Pressure Sensor," Sixth International Conference on Automotive Electronics, 82-6, 1987.
47. Kawamura, Y., et al., "MBT Control through Individual Cylinder Pressure Detection," SAE Paper 881779, 1988.
48. Laubenstein, C., et al., "Peak Cylinder Combustion Pressure Ignition Spark Timing System," US Patent 4,153,019, May 8, 1979.
49. Hubbard, M., Dobson, P., and Powell, D., "Closed Loop Control of Spark Advance Using a Cylinder Pressure Sensor," Journal of Dynamic Systems, Measurement, and Control, December 1976.
50. Powell, D., Hubbard, D., Clappier, R., "Ignition Timing Control Method and Apparatus," US Patent 4,063,538, Dec. 20, 1977.
51. Glaser, I., and Powell, D., "Optimal Closed-Loop Spark Control of an Automotive Engine," SAE Paper 810058, 1981.
52. Matekunas, F., "Spark-Ignition Engines – Combustion Characteristics, Thermodynamics, and the Cylinder Pressure Card", General Motors Research Publication GMR-4660. Central States Section of the Combustion Institute, March, 1984.
53. Matekunas, F., "Modes and Measures of Cyclic Combustion Variability", SAE Paper 830337, 1983.
54. Inoue, T., et al., "Toyota Lean Combustion System – The Third Generation System," SAE Paper 930873, 1993.
55. Kobayashi, N., et al., "Development of the Toyota Lean Combustion System", JSAE Review, p. 106, July 1984.
56. Watanabe, S., et al., "A Sophisticated Engine Control System Using Combustion Pressure Detection", SAE Paper 960042, 1996.
57. Hamburg, D.R., Hogh, G., and Lawson, G.P., "Adaptive Lean Limit Air-Fuel Control Using Combustion Pressure Sensor Feedback", US Patent 4,736,724, 1988.
58. Mortara, W., and Canta, C., "Engine Stability Sensor", SAE Paper 830428, 1983.
59. Morita, et al., "Air/Fuel Ratio Control System for Internal Combustion Engine and Method Therefore", US Patent 4,543,934, 1985.
60. Gilkey, J., "Fuel-Air Ratio Estimation from Cylinder Pressure in an Internal Combustion Engine," Phd. Thesis, Standford University, August, 1984.
61. Gilkey, J., and Powell, D., "Fuel-Air Ratio Estimation from Cylinder Pressure Time Histories," J. of Dynamic Systems, Measurement, and Control, Dec. 1985.
62. Gassenfeit, E., and Powell, D., "Algorithms for Air-Fuel Ratio Estimation Using Internal Combustion Engine Cylinder Pressure," SAE Paper 890300, 1989.
63. Rohde-Brandenburger, K., "Einfluss des Zundwinkels auf den Wirkungsgrad eines Mehrzylinder-Ottomotors im instationaren Betrieb VDI fortschritt-Berichte, Reihe 12, Nr. 79 (1986).
64. Kleinschmidt, P., and Von Garssen, H., "Process for Producing a Control Signal for the Ignition Point of an Internal Combustion Engine", German Patent No. DE 4318504 C1, October 27, 1994.
65. Hosey, R., and Powell, D., "Closed Loop Knock Adaptive Spark Timing Control Based on Cylinder Pressure," ASME Winter Meeting, 1978.
66. Schmillen, K.P., and Rechs, M., "Different Methods of Knock Detection and Knock Control", SAE Paper 910858, 1991.
67. Checkel, M.D., and Dale, J.D., "Computerized Knock Detection from Engine Pressure Records", SAE Paper 860028, 1986.
68. Rassweiler, G.M., and Withrow, L., "Motion Pictures of Engine Flames Correlated with Pressure Cards", SAE Journal (Trans), Vol. 42, pg. 185-204, May 1938 (Reprinted SAE Paper 800131, 1980).
69. Matekunas, F., "Engine Combustion Control with Ignition Timing by Pressure Management Ratio," US Patent No. 4,622,939, Nov. 18, 1986.
70. Matekunas, F., "Engine Combustion Control with Dilution Flow by Pressure Management Ratio," US Patent No. 4,624,229, Nov. 25, 1986.
71. Matekunas, F., "Engine Combustion Control with Fuel Balancing by Pressure Management Ratio," US Patent No. 4,621,603, Nov. 11, 1986.
72. Sellnau, M.C., "Combustion Pressure Sensor," US Patent 4,969,352, November 13, 1990.
73. Sellnau, M.C., "Non-Intrusive Cylinder Pressure Sensor," US Patent 5,329,809, July 19, 1994.
74. Sellnau, M.C., "Non-Intrusive Cylinder Pressure Sensor Having Improved Response Characteristics," US Patent 5,367,904, November 29, 1994.

CONTACT

Mark Sellnau is a Senior Staff Research Engineer working in the Combustion and Engine Systems Group at Delphi R&D. He was formerly employed at GM Research Labs for over 14 years in the areas of cylinder-pressure-based engine control, engine combustion and emissions, and advanced engine technologies. He holds 6 patents in the field.

He received a degree of Bachelors of Science in Mechanical Engineering at the Univ. of Michigan, Ann Arbor; and a Masters of Science in Mechanical Engineering at MIT.

For additional information, contact this author at:

Mark Sellnau
810-986-0902
mark.sellnau@delphiauto.com
Delphi Central Research and Development
M/C 480-106-104
30500 Mound Rd.
Warren, MI 48090

Frederic Matekunas is a Senior Staff Research Engineer working in technology assessment at GM R&D and Planning. He has been employed at GM for 26 years working in the field of engine combustion and powertrain control. He holds five patents and one Horning Award.

He received a Bachelors of Science in Mechanical Engineering (1968), a Masters of Science in Mechanical Engineering (1971), and a Doctorate in Mechanical Engineering (1973) at Purdue University.

For additional information, contact this author at:

Frederic Matekunas
810-986-2904
frederic.a.matekunas@gm.com
GM R&D and Planning
M/C 480-106-336
30500 Mound Rd.
Warren, MI 48090

NOMENCLATURE

A/F: Air-Fuel ratio
ATDC: After-Top-Dead-Center
C: Centigrade
CAD: Crank-Angle-Degrees
COV: Coefficient of Variation
DB: Decibels
DC: Direct Current
DILPAR: PRM Dilution Parameter
DLD: Dilution Limit Detection
DOHC: Double-Over-Head-Cam
DP: Differential Pressure
DPI: Differential Pressure Integral
ECU: Engine Control Unit
EGR: Exhaust Gas Recirculation
EMC: Electromagnetic Compatibility
ESD: Electrostatic Discharge
FET: Field Effect Transistor
FPR: Final Pressure Ratio
FTP: Federal Test Procedure
FS: Full Scale
HC: Hydrocarbon Emissions
IMEP: Indicated Mean Effective Pressure
JFET: Junction FET
KHz: Kilohertz
LPP: Location of Peak Pressure
MBF: Mass Burn Fraction
MBT: Minimum Spark Advance for Best Torque
MOSFET: Metal Oxide Semiconductor FET
Mpa: Megapascals
MPR: Modified Pressure Ratio
OBDII: On-Board Diagnostics II

O₂: Exhaust Oxygen
N: Newtons
NJFET: N-type Junction FET
Nox: Nitric Oxide Emissions
P: Cylinder Pressure
P_{mot}: Motoring Cylinder Pressure
PR: Pressure Ratio
PRM: Pressure Ratio Management
PRM10: PRM Timing Parameter
SMT: Surface Mount Technology
SPB: Spark Plug Boss Sensor
SPICE: Simulation Program with Integrated Circuit Emphasis
TCD: Total Charge Dilution
TDC: Top-Dead-Center
θ: Crank-Angle-Position